ELSEVIER

Journal of Biomechanics 40 (2007) 3476–3486

JOURNAL OF BIOMECHANICS

www.elsevier.com/locate/jbiomech
www.JBiomech.com

Pulse wave propagation in a model human arterial network: Assessment of 1-D numerical simulations against *in vitro* measurements

Koen S. Matthys[a], Jordi Alastruey[a,b], Joaquim Peiró[a], Ashraf W. Khir[c], Patrick Segers[d], Pascal R. Verdonck[d], Kim H. Parker[b], Spencer J. Sherwin[a,*]

[a]*Department of Aeronautics, Imperial College London, London, UK*
[b]*Department of Bioengineering, Imperial College London, London, UK*
[c]*School of Engineering and Design, Brunel University, Uxbridge, Middlesex, UK*
[d]*Cardiovascular Mechanics and Biofluid Dynamics (CMBD) Research Unit, Institute of Biomedical Technology, Ghent University, Belgium*

Accepted 28 May 2007

Abstract

A numerical model based on the nonlinear, one-dimensional (1-D) equations of pressure and flow wave propagation in conduit arteries is tested against a well-defined experimental 1:1 replica of the human arterial tree. The tree consists of 37 silicone branches representing the largest central systemic arteries in the human, including the aorta, carotid arteries and arteries that perfuse the upper and lower limbs and the main abdominal organs. The set-up is mounted horizontally and connected to a pulsatile pump delivering a periodic output similar to the aortic flow. Terminal branches end in simple resistance models, consisting of stiff capillary tubes leading to an overflow reservoir that reflects a constant venous pressure. The parameters required by the numerical algorithm are directly measured in the *in vitro* set-up and no data fitting is involved. Comparison of experimental and numerical pressure and flow waveforms shows the ability of the 1-D time-domain formulation to capture the main features of pulse wave propagation measured throughout the system test. As a consequence of the simple resistive boundary conditions used to reduce the uncertainty of the parameters involved in the simulation, the experimental set-up generates waveforms at terminal branches with additional non-physiological oscillations. The frequencies of these oscillations are well captured by the 1-D model, even though amplitudes are overestimated. Adding energy losses in bifurcations and including fluid inertia and compliance to the purely resistive terminal models does not reduce the underdamped effect, suggesting that wall visco-elasticity might play an important role in the experimental results. Nevertheless, average relative root-mean-square errors between simulations and experimental waveforms are smaller than 4% for pressure and 19% for the flow at all 70 locations studied.

Keywords: Pulse wave propagation; Experimental modelling; One-dimensional modelling; Time-domain formulation; Bifurcating network of vessels

1. Introduction

A profound understanding of pressure and flow pulse wave propagation in the cardiovascular system and of the impact of disease and anatomical variations on these propagation patterns can provide valuable information for clinical diagnosis and treatment (Cruickshank et al., 2002; Blacher and Safar, 2005; Fujimoto et al., 2004). Computational arterial models are playing an increasingly significant role in current vascular research (Taylor and Draney, 2004). Models can simulate wave propagation in an accurate, fast and reproducible manner in vessel locations and under patient conditions that cannot be assessed *in vivo*. Through modelling, insight can be obtained into the relation between healthy or pathological blood pressure and flow waveforms and various underlying cardiac and vessel parameters, such as heart rate, cardiac output, arterial wall geometry, distensibility and peripheral impedance to the flow. This knowledge then permits the evaluation of the impact of specific and localised treatment.

Despite growing interest in three-dimensional (3-D) simulations, a one-dimensional (1-D), time-domain approach also provides important, although different

*Corresponding author. Tel.: +44 20 7594 5052; fax: +44 20 7584 8120.
E-mail address: s.sherwin@imperial.ac.uk (S.J. Sherwin).

0021-9290/$ - see front matter © 2007 Elsevier Ltd. All rights reserved.
doi:10.1016/j.jbiomech.2007.05.027

insights into cardiovascular physiology (Wan et al., 2002; Sherwin et al., 2003a; Franke et al., 2003; Formaggia et al., 2006; Alastruey et al., 2006, 2007b). Typically, 3-D models are limited to local areas of the arterial system, mainly because of their high computational cost, while 1-D models offer a good compromise between accuracy and cost when a more global assessment of the system can suffice. In interventional planning procedures, 3-D models are becoming increasing popular, while 1-D models are better suited for assessing wave morphology and propagation patterns as an aid to pharmacological treatment. For the future, the large range of scales within the cardiovascular system suggests the use of a multiscale modelling approach involving the interaction and coupling between 3-D, 1-D and 0-D models, as has been advocated by Formaggia et al. (2001).

An accurate, quantitative testing of the 1-D formulation against *in vivo* data is complicated because some of the elastic and geometrical properties of the arterial system are very difficult to measure without highly invasive procedures. Previous *in vivo* validations have been presented in Olufsen et al. (2000) and Steele et al. (2003), but they involved some parameter fitting (Olufsen et al., 2000) or considered only a local part of the system (Steele et al., 2003). We have previously tested the 1-D formulation against measurements in the aorta of a well-defined 1:1 *in vitro* model of the large conduit arteries of the systemic circulation (Segers et al., 1998) using the linear, frequency-based formulation (Segers and Verdonck, 2000) and the nonlinear, time-domain formulation (Alastruey, 2006). In this work, we test the nonlinear, time-domain formulation in both aortic *and* peripheral locations using a new 1:1 *in vitro* silicone model in which all the parameters involved in the simulation can be accurately measured. The effects on pulse wave propagation of energy losses at bifurcations and the fluid inertia and wall compliance of the outflow conditions are also studied.

2. Methodology

From the experimental model we obtain the geometrical and material properties of the arterial network, the rheological data of the test fluid and the inflow and outflow boundary conditions. Pressure and flow measurements are taken at 70 locations along the whole network. The data obtained just distal to the aortic valve and at the terminal locations are used as boundary conditions in the numerical model. The remaining data are treated as comparative data for the pressure and flow waveforms simulated with the numerical model.

2.1. Experimental model

2.1.1. Set-up

The experimental model is a 1:1 replica of the 37 largest conduit arteries of the systemic circulation and mimics three generations of bifurcating branches (Fig. 1). The network was manufactured using in-house crafted

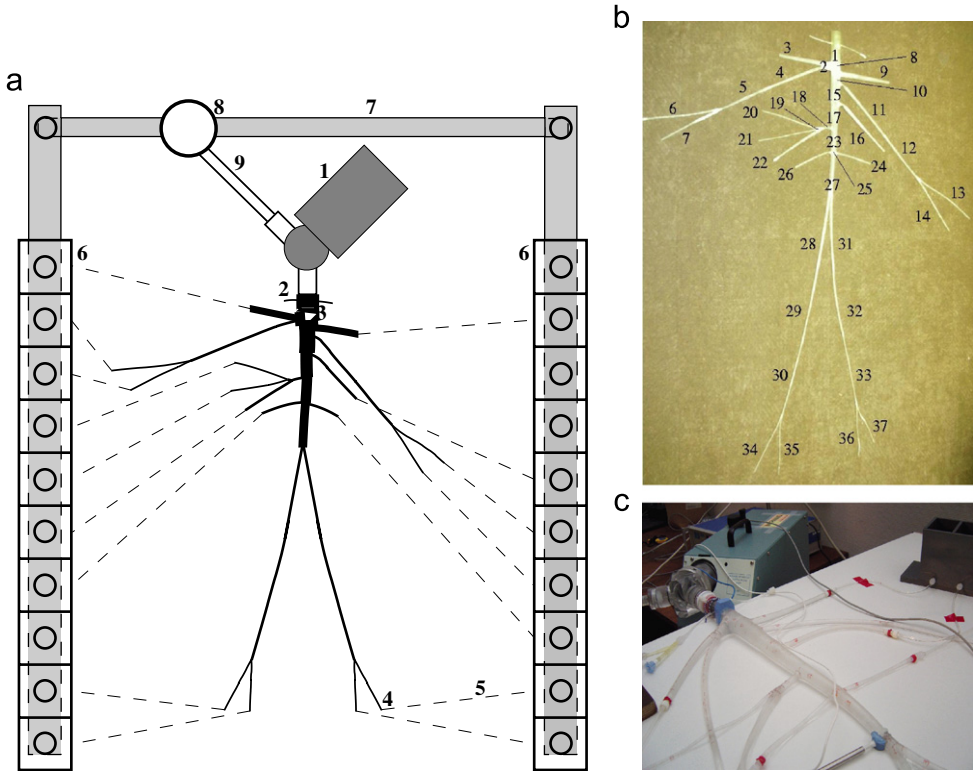

Fig. 1. (a) Planview schematic of the hydraulic model. 1: Pump (left heart); 2: catheter access; 3: aortic valve; 4: peripheral resistance tube; 5: stiff plastic tubing (veins); 6: venous overflow; 7: venous return conduit; 8: buffering reservoir; 9: pulmonary veins. (b) The 37 arteries simulated. (c) Detail of the pump and the aorta.

tubular aluminium moulds (CMBD Research Unit, Ghent University, Belgium), which were either linearly tapered or had constant cross-section (for the smallest branches). A two-component silicone material (Baysilone LSR2050, General Electric, Fairfield, CT, USA) was hand-painted in six layers on each mould. Curing between subsequent layers was done at 150 °C. The silicone network was manually assembled piece by piece, mounted horizontally and subsequently connected proximally to a Harvard pulsatile pump providing for a periodic input flow, and distally to a set of terminal resistance tubes connected to overflow reservoirs, creating a closed loop hydraulic system. A 65–35% water–glycerol mixture, with density $\rho = 1050\,\mathrm{kg\,m^{-3}}$ and viscosity $\mu = 2.5\,\mathrm{mPa\,s}$ at 30 °C, was used to mimic the density and viscous properties of blood.

2.1.2. Protocol

Values of length, radius and wall thickness were measured at the inlet, middle point and outlet of each arterial segment (Fig. 1b) using a ruler, callipers and micrometer. These measurements were taken at the end of the experiment and after having dissected the model. The elastic wall properties were measured by performing a tensile test on 63 silicone sample strips, taken from specimen sheets of various thicknesses and angles with respect to the principal direction of painting the silicone layers. A constant Young's modulus of 1.2 MPa was measured within the working interval of pressures of the experiment.

Inflow conditions were imposed by the Harvard pump with the following settings: 70 beats per minute (with a systole-to-diastole ratio of 35/65) and a stroke volume of 70 ml, creating a mean pressure of approximately 100 mmHg at the aortic root. Outflow boundary conditions were determined by passive resistance elements, made of a single flexible plastic tube (length 250 mm; Ø2 mm) and an overflow reservoir, inducing a back pressure of 3.2 mmHg. Peripheral compliances were not included in this experimental model. The simplicity of this type of outlet allowed accurate quantification of its parameters, although it induced some non-physiological features in the pressure and flow waveforms (see Section 4).

The flow rate was measured using an ultrasonic volume flow meter (Dual Channel Flowmeter, Transonic Systems Inc., Ithaca, NY, USA) with five different sized probes (Transonic Flowprobe Ø24, Ø16, Ø12, Ø8 and Ø3 mm). Pressure was measured simultaneously by means of two micro-tip catheter pressure transducers (Millar Instruments, Houston, TX, USA). Peripheral recording of the pressure and flow was always accompanied by a simultaneous measurement of the pressure and flow just distal to the aortic valve. Measurements were taken at 70 sites along the arterial network, including the six locations in the aorta originally studied by Segers et al. (1998).

2.1.3. Data acquisition and analysis

At the start of the experiment, pressure sensors were calibrated against a water column while flow sensors were tested via comparison with volumetric flow measurements. Calibration readings were also taken at regular intervals to allow for thermal drift correction during post-processing. The signals of the two pressure transducers were connected to an in-house signal-conditioning unit. The signals of the dual flow meter were indirectly connected to the same unit, passing first through the transonic flow meter system. The amplified signals were sampled at 1000 Hz and sent to a PC via a 12-bit multifunction I/O DAQ card (National Instruments, Austin, TX, USA). The acquisition software is an in-house program, written in LabVIEW.

At least 10 successive beats of pressure and the flow were recorded at each measurement location. The data analysis was performed, off-line, in Matlab. The signals were first calibrated and subsequently filtered with a fifth order low-pass (20 Hz) Butterworth filter to reduce noise on the signals while maintaining the relevant frequency information. Subsequently, a minimum of eight beats were selected from the recorded beats and ensemble averaged to generate a single beat pressure and flow waveform to be compared with their numerical counterparts.

2.2. Numerical model

2.2.1. Governing equations

The 1-D governing equations result from conservation of mass and balance of momentum applied to a 1-D impermeable and deformable tubular control volume of incompressible and Newtonian fluid. Following Smith et al. (2001) and Sherwin et al. (2003b), they take the form

$$\frac{\partial A}{\partial t} + \frac{\partial (AU)}{\partial x} = 0, \tag{1}$$

$$\frac{\partial U}{\partial t} + U\frac{\partial U}{\partial x} + \frac{1}{\rho}\frac{\partial p}{\partial x} = \frac{f}{\rho A}, \tag{2}$$

where x is the axial coordinate along the vessel, t is time, $A(x,t)$ is the cross-sectional area of the vessel, $U(x,t)$ is the average axial velocity of the fluid, $p(x,t)$ is the average internal pressure over the cross-section and $f(x,t)$ is the friction force per unit length. We consider $f = -22\mu\pi U$, which was obtained by fitting experimental data measured at different points in the cardiac cycle to an axisymmetric and constant velocity profile that satisfies the no-slip condition (Smith et al., 2001).

The system of governing equations can be completed with the pressure–area relation previously used in Olufsen et al. (2000), Sherwin et al. (2003a, b), Franke et al. (2003), Alastruey et al. (2006, 2007a, b). It assumes a thin, homogeneous and elastic arterial wall and it takes the form

$$p = p_0 + \frac{\beta}{A_0}(\sqrt{A} - \sqrt{A_0}), \quad \beta = \frac{\sqrt{\pi}hE}{(1-\sigma^2)}, \tag{3}$$

where $\beta(x)$ represents the elastic properties of the vessel wall, which depend on the sectional area, $A_0(x)$, and wall thickness, $h(x)$, at the reference state $(p, U) = (p_0, 0)$, the Young's modulus, $E(x)$, and the Poisson's ratio, σ, taken to

be $\sigma = \frac{1}{2}$ as the wall is assumed to be incompressible. Although Eq. (3) considers a non-physiological linear relation between changes in pressure and changes in cross-sectional radius, it approximates the distensibility of the silicone wall for the range of working pressures, according to the tensile tests described in Section 2.1.2. The parameter β is related to the speed of pulse wave propagation, $c(x,t)$, through (Sherwin et al., 2003b)

$$c^2 = \frac{\beta}{2\rho A_0} A^{1/2}. \quad (4)$$

2.2.2. Numerical scheme

The solutions of Eqs. (1)–(3) are pressure and flow waves that are reflected at the junctions and terminal resistances and due to the effect of tapering. Therefore, it is important that the numerical method can propagate waves of different frequencies without suffering from excessive dispersion and diffusion errors. This can be achieved with a spectral/*hp* discontinuous Galerkin scheme that involves the solution of Riemann problems at the interfaces within each artery, at the boundaries and at the junctions. A second-order Adams–Bashforth scheme is used for the time-integration. Details on this algorithm can be found in Karniadakis and Sherwin (2003), Sherwin et al. (2003b) and Alastruey (2006).

Table 1 shows the data used in the 1-D simulation, which were directly measured from the experimental set-up (see Sections 2.1.2 and 4.1). Wave speed values are calculated using Eq. (4) with the Young's modulus obtained from a tensile test. We initially assume $A(x,0) = A_0(x)$ and $U(x,0) = 0$ in all the silicone tubes, and run the model until it converges to a periodic solution. This takes about 10 cardiac cycles and of the order of 5 min to run on a standard PC.

Table 1
Data of the 37 silicone tubes shown in Fig. 1b

Arterial segment	l (mm)±2.0%	$R_{in} \rightarrow R_{out}$ (mm)±3.5%	h (mm)±2.5%	$c_{in} \rightarrow c_{out}$ (m/s)	R_p (10^9 Pa s m^{-3})
(1) Ascending aorta	36	14.40 → 13.00	0.51	5.21 → 5.49	–
(2) Innominate	28	11.00 → 7.29	0.35	4.89 → 6.01	–
(3) R. carotid	145	5.37 → 3.86	0.28	6.35 → 7.49	2.67
(4) R. subclavian I	218	4.36 → 3.34	0.27	6.87 → 7.84	–
(5) R. subclavian II	165	3.34 → 2.78	0.16	6.00 → 6.58	–
(6) R. radial	235	2.07	0.15	7.43	3.92
(7) R. ulnar	177	2.10	0.21	8.81	3.24
(8) Aortic arch I	21	13.00 → 12.50	0.50	5.41 → 5.52	–
(9) L. carotid	178	5.58 → 3.73	0.31	6.55 → 8.00	3.11
(10) Aortic arch II	29	12.50 → 11.80	0.41	4.98 → 5.12	–
(11) L. subclavian I	227	4.42 → 3.39	0.22	6.21 → 7.10	–
(12) L. subclavian II	175	3.39 → 2.84	0.17	6.26 → 6.84	–
(13)L. radial	245	2.07	0.21	8.84	3.74
(14) L. ulnar	191	2.07	0.16	7.77	3.77
(15) Thoracic aorta I	56	11.80 → 11.00	0.43	5.29 → 5.48	–
(16) Intercostals	195	4.12 → 3.22	0.27	7.07 → 7.99	2.59
(17) Thoracic aorta II	72	11.00 → 9.26	0.34	4.84 → 5.26	–
(18) Celiac I	38	3.97	0.20	6.20	–
(19) Celiac II	13	4.31	1.25	14.90	–
(20) Splenic	191	1.83	0.13	7.24	3.54
(21) Gastric	198	1.92	0.11	6.73	4.24
(22) Hepatic	186	3.31 → 2.89	0.21	6.95 → 7.44	3.75
(23) Abdominal aorta I	62	9.26 → 8.01	0.33	5.19 → 5.59	–
(24) L. renal	120	2.59	0.19	7.39	3.46
(25) Abdominal aorta II	7	7.90	0.35	5.83	–
(26) R. renal	118	2.55	0.16	6.95	3.45
(27) Abdominal aorta III	104	7.80 → 5.88	0.30	5.41 → 6.24	–
(28) R. iliac-femoral I	205	3.90 → 3.38	0.21	6.47 → 6.94	–
(29) R. iliac-femoral II	216	3.38 → 2.31	0.15	5.89 → 7.13	–
(30) R. iliac-femoral III	206	2.31 → 2.10	0.20	8.04 → 8.44	–
(31) L. iliac-femoral I	201	4.02 → 3.34	0.20	6.19 → 6.79	–
(32) L. iliac-femoral II	195	3.34 → 2.26	0.16	6.11 → 7.44	–
(33) L. iliac-femoral III	207	2.26 → 2.12	0.13	6.67 → 6.89	–
(34) R. anterior tibial	163	1.55	0.15	8.47	5.16
(35) R. posterior tibial	151	1.53	0.12	7.73	5.65
(36) L. posterior tibial	149	1.58	0.11	7.23	4.59
(37) L. anterior tibial	126	1.55	0.10	7.01	3.16

l: length; $R_{in} \rightarrow R_{out}$: diastolic cross-sectional radii at the inlet and the outlet; h: average wall thickness; $c_{in} \rightarrow c_{out}$: wave speed at the inlet and the outlet; R_p: peripheral resistance. Single numbers indicate vessels with a constant cross-section. The interval of confidence of the geometrical measurements is indicated in the heading.

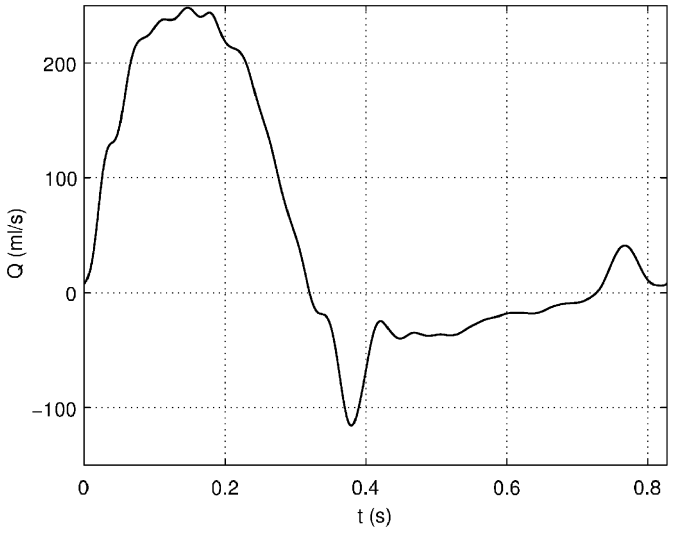

Fig. 2. The experimental flow rate measured at the ascending aorta is enforced as the inflow boundary condition of the simulations.

2.2.3. Treatment of boundary conditions and bifurcations

The hyperbolic system of partial differential equations (1) and (2) with the pressure–area relationship (3) is solved in each silicone tube of Fig. 1b using the following boundary conditions. At the inlet of the ascending aorta, the flow measured in the experiment and ensemble averaged (Fig. 2) is enforced as a periodic inflow boundary condition. The plastic tube attached to the outlet of each terminal branch and the overflow reservoir at constant height are simulated as outflow boundary conditions by enforcing the relation

$$Q_{1D} = \frac{p_{1D} - p_{out}}{R_p}, \tag{5}$$

where Q_{1D} and p_{1D} are the flow rate and pressure at the outlet of the 1-D terminal branch, $p_{out} = 3.2$ mmHg is the constant hydrostatic pressure measured at the overflow reservoir and R_p is the peripheral resistance to the flow, determined from mean pressure and flow measurements close to the outlet of each terminal branch. The values of R_p are shown in the last column of Table 1. Combined, they yield a total peripheral resistance of 2.25×10^8 Pa s m^{-3}. Applying Eq. (5) with Q_{1D} and p_{1D} as the mean experimental flow rate and pressure measured at the inlet of the ascending aorta produces a larger total resistance (2.37×10^8 Pa s m^{-3}), since it consists of the total peripheral resistance plus the effect of viscous dissipation throughout the vessels and junctions of the system within the 37 arterial segments.

Boundary conditions of the arterial segments joining at junctions are prescribed by enforcing conservation of mass and continuity of the total pressure $p + \frac{1}{2}\rho U^2$ (the effect of energy losses is analysed in Section 3.2). A more detailed description of the treatment of boundary conditions and junctions can be found in Sherwin et al. (2003b) and Alastruey (2006).

3. Results

Section 3.1 compares the experimental pressure and flow waveforms with the numerical predictions obtained using the geometry, elasticity and boundary conditions measured in the silicone network. It is important to stress that none of the parameters involved in the simulation have been tuned, except for phase matching the onset of the experimental and numerical systolic ejections during data post-processing. We also analyse the effect on pulse waveforms of simulating energy losses at bifurcations (Section 3.2) and the fluid inertia and wall compliance of the peripheral plastic tubes (Section 3.3), with particular emphasis on the peripheral vessels.

3.1. Comparison between experimental and numerical results

Fig. 3 compares experimental and numerical pressure and flow waveforms at three representative locations along the silicone aorta, showing the ability of the 1-D formulation to capture the main features of aortic pulse wave propagation. Despite the simple terminal boundary conditions used, the experimental model is able to reproduce the main features of pressure and the flow observed *in vivo*, such as the dicrotic notch, diastolic decay and peaking and steepening of pulse pressure as we move away from the heart (Caro et al., 1978). We also observe the presence of some backward flow after the closure of the two-leaflet aortic valve, and a reduction in the amplitude of the flow with the distance from the heart. The good match observed at the aortic tubes highlights the relative independence of the pulse waveform from the terminal boundary conditions, which was to be expected from our network since the junctions are well-matched for forward waves.

Typical comparisons between experimental and numerical results in the rest of the vessels of the system are shown in Figs. 4–6. Each figure compares experimental and numerical results in representative vessels of each generation of bifurcations, going from vessels branching off the experimental aorta (Fig. 4) to vessels of the third generation of bifurcations (Fig. 6). We observe that the 1-D formulation is able to predict the essential characteristics of the *in vitro* pressure and flow waveforms in the rest of the vessels simulated. Due to the simple resistance boundary conditions used in the experiment, the measured pulse waves become less physiological in the more distal vessels. They contain many non-physiological oscillations, in both pressure and the flow, whose frequency is surprisingly well captured by the 1-D model. However, the amplitude of the numerical oscillations is higher than the amplitude of their experimental counterparts. We note that peripheral reflected waves do not have a significant effect on the aortic flows, because they get 'trapped', on their way to the aorta, at the junctions of our network, which are not well-matched for backward travelling waves.

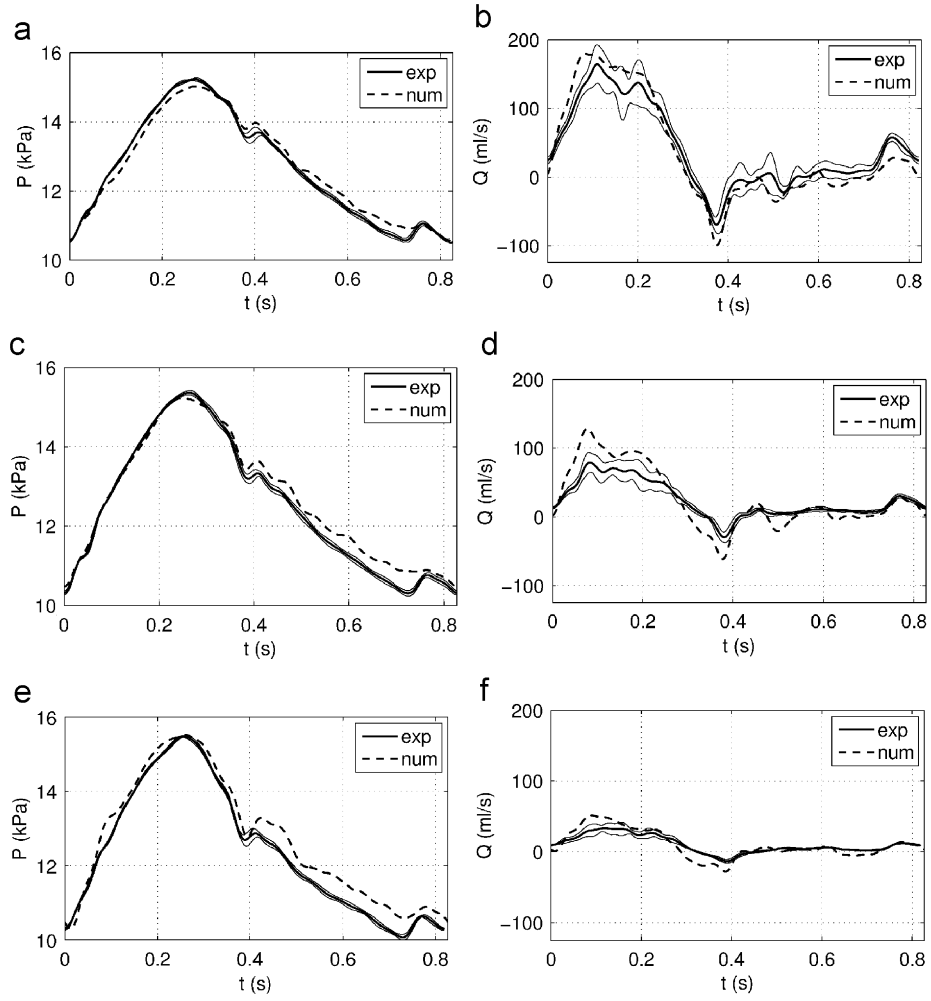

Fig. 3. Experimental and theoretical pressure (left) and flow (a,b) waveforms: (top) aortic arch II (segment 10 in Table 1), (c,d) thoracic aorta II (segment 17) and (e,f) abdominal aorta III (segment 27). The figures also show the standard deviation (thin solid lines) of the ensemble averaged of each experimental measurement.

To study the accuracy of the numerical predictions, a root-mean-square error defined as $\overline{\mathscr{E}} = \sum \sqrt{\mathscr{X}^2}/N$, is calculated in each measuring location. The sum is over the cardiac cycle, $\mathscr{X}(t)$ is the difference between experimental and numerical instantaneous pressures or flow samples, and N is the number of samples. Discrepancies between the experimental and numerical mean pressure or flow values are also determined for each measuring location. Table 2 shows the average value of these errors (expressed relative to the local maximum of the experimental pressure or flow values) at all of the measurement sites along the aorta and in the vessels of the first, second and third generation of bifurcations. Average relative errors between simulations and experimental waveforms are smaller than 4% for pressure and 19% for the flow at all 70 locations studied. The larger relative errors of flow predictions compared to pressure predictions are consistent with the larger uncertainty in the experimental flow measurements compared to the experimental pressure measurements (see the standard deviations in Figs. 3–6).

If the convective term is neglected from Eq. (2) and Eq. (3) is linearised as $p = (\beta/2A_0^{3/2})(A - A_0)$, the simulated pulse pressures are larger, because the arterial network is less compliant (Fig. 7). Moreover, the linear formulation is worse at capturing the phase of the reflected waves from the experiment. However, average relative errors between simulations and experimental waveforms are still smaller than 4% for pressure and 19% for the flow at all 70 locations studied, which suggests that the effect of nonlinearities on waveforms is only secondary under the conditions of the experiment. This is in agreement with our previous result in Sherwin et al. (2003b).

3.2. Effect of energy losses at bifurcations on the simulation

Energy losses at bifurcations can be modelled by adding a loss coefficient into the continuity of the total pressure $p + \frac{1}{2}\rho U^2$. The value of the loss coefficient at each bifurcation is determined using the semi-empirical model proposed by Gardel (1957a, b), which takes into account

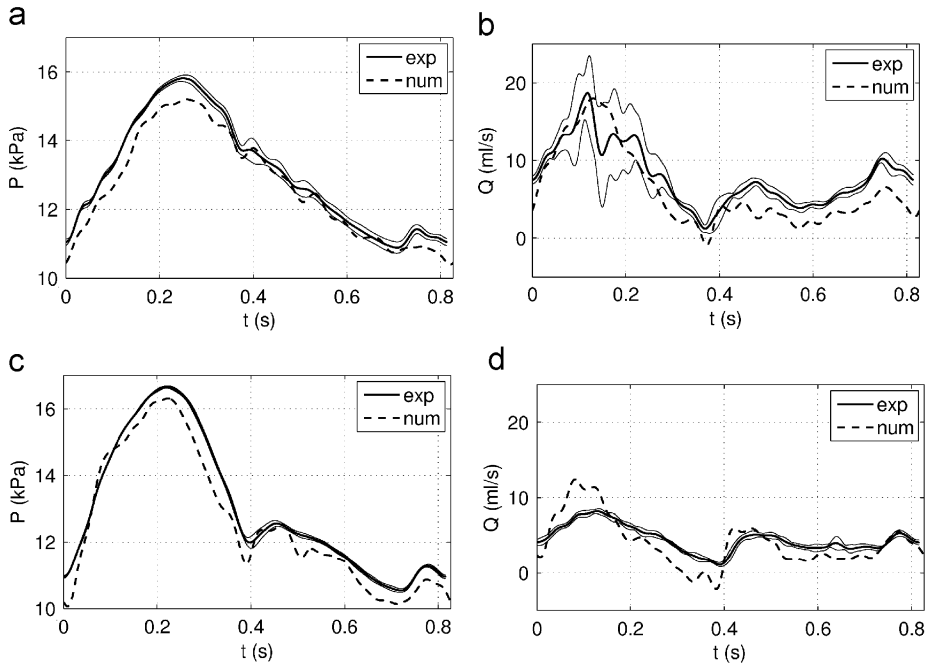

Fig. 4. Experimental and theoretical pressure (left) and flow (right) waveforms in typical first generation vessels: (a,b) left subclavian I (segment 11), (c,d) right iliac-femoral II (segment 29). The figures also show the standard deviation (thin solid lines) of the ensemble averaged of each experimental measurement.

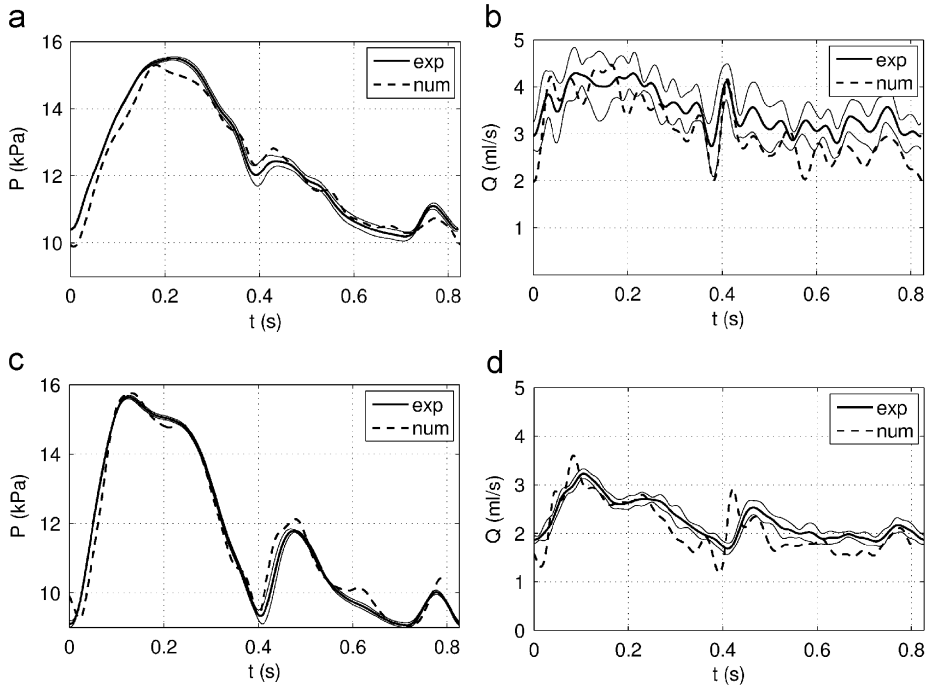

Fig. 5. Experimental and theoretical pressure (left) and flow (right) waveforms in typical second generation vessels: (a,b) left ulnar (segment 14), (c,d) right anterior tibial (segment 34). The figures also show the standard deviation (thin solid lines) of the ensemble averaged of each experimental measurement.

the branching angles and the flow and area ratios of the vessels joining at the bifurcation. Although this method assumes rigid vessel walls, to our knowledge it is the best approximation to determine energy losses in 1-D pulsatile flows. Steele et al. (2003) have also applied this model to simulate pulse wave propagation in a porcine arterial bypass.

The addition of these loss coefficients in our simulations does not have a significant effect on pressure and flow waveforms. Differences between a model with and without

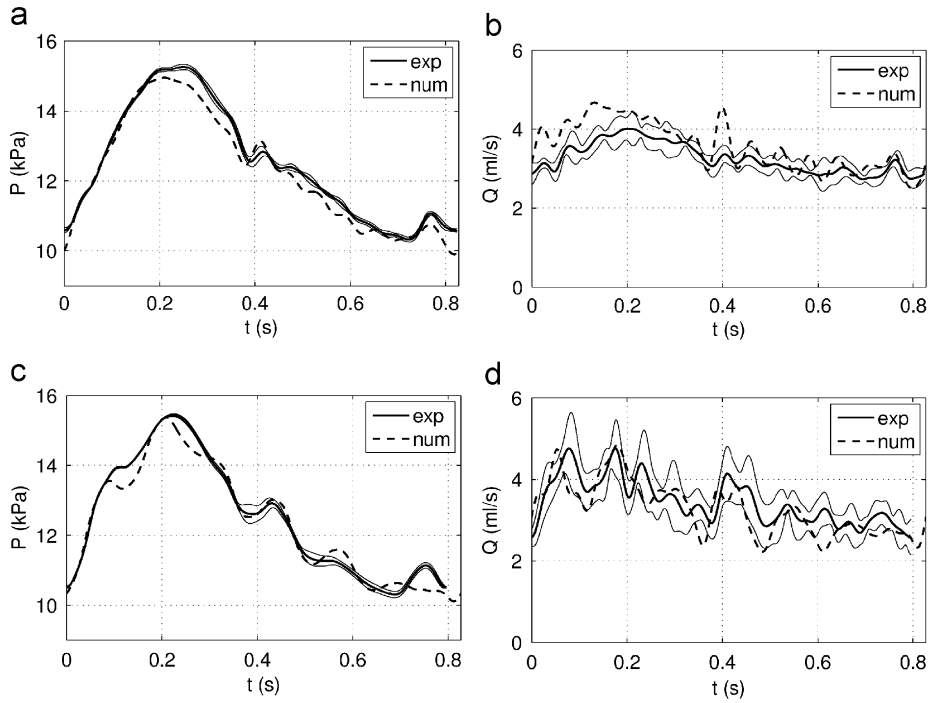

Fig. 6. Experimental and theoretical pressure (left) and flow (right) waveforms in typical third generation vessels: (a,b) right ulnar (segment 7), (c,d) splenic (segment 20). The figures also show the standard deviation (thin solid lines) of the ensemble averaged of each experimental measurement.

Table 2
Average relative errors of the numerical pressures and flows in all the vessels of the aorta and the first, second and third generation of bifurcations

Measuring location	$\mathscr{E}$ pressure (%)	$\mathscr{E}$ flow (%)	$\overline{p}$ (%)	$\overline{Q}$ (%)
Aorta	1.5	13.6	1.2	2.3
First generation	3.4	18.8	2.9	9.7
Second generation	3.4	15.8	2.9	5.9
Third generation	2.2	11.3	1.5	6.8

The second and third columns show the relative root-mean-square errors, $\mathscr{E}$, as defined in the text, and the last two columns show the relative errors of the mean pressure, $\overline{p}$, and mean flow rates, $\overline{Q}$. All errors are expressed relative to the local maximum of the experimental pressures or flow rates.

energy losses cannot be noted in the scale of Figs. 3–6. The main effect is a change in the mean pressures and flows by less than 0.5%. The mean pressure at the root of the network is 0.2% larger when energy losses are simulated, since the same amount of fluid has to be pumped through a more resistant network. According to these results, we observe that energy losses at bifurcations have a secondary effect on blood flow in large arteries, and cannot explain the higher amplitudes of the numerical oscillations in peripheral branches.

3.3. Effect of terminal models on the simulation

In the simulations above, the plastic tubes attached to each terminal silicone branch were modelled as pure resistors through Eq. (5). In this section we analyse the effect of fluid inertia and wall compliance in the resistance tubes on the predictions of the 1-D model. Peripheral fluid inertia is included in the resistive outflows by coupling an LR model, consisting of an inductance L and a resistance R_p, to the outlet of each 1-D terminal branch. This model (Alastruey, 2006) is governed by

$$L\frac{dQ_{1D}}{dt} + R_p Q_{1D} + p_{out} - p_{1D} = 0, \tag{6}$$

with $L = \rho l/A_0$ ($l = 250\,\text{mm}$ is the length of the plastic tube and $A_0 = \pi\,\text{mm}^2$ is its cross-sectional area). The effect of any possible peripheral compliance is simulated by coupling an RCR model consisting of two resistances, R_1 and R_2 ($R_1 + R_2 = R_p$), and a compliance, C, in between them. This model (Alastruey, 2006) is governed by

$$p_{1D} + R_2 C\frac{dp_{1D}}{dt} = p_{out} + (R_1 + R_2)Q_{1D} + R_1 R_2 C\frac{dQ_{1D}}{dt}. \tag{7}$$

According to the study in Alastruey et al. (2007a), we consider $R_1 = \rho c_0/A_0$, with $c_0 = c(A_0)$ given by (4), to allow any incoming wave from the 1-D terminal branch to reach C and R_2 without being reflected by R_1. The compliance C of each RCR model is taken to be $10^{-11}\,\text{m}^3\,\text{Pa}^{-1}$. Eqs. (6) and (7) are solved using a first-order time discretisation.

Fig. 8 shows the effect of simulating the terminal boundary conditions with either the LR or RCR models on the pressure and flow time histories predicted in the left renal vessel. The addition of the peripheral fluid inertia increases the amplitude of the pressure and flow

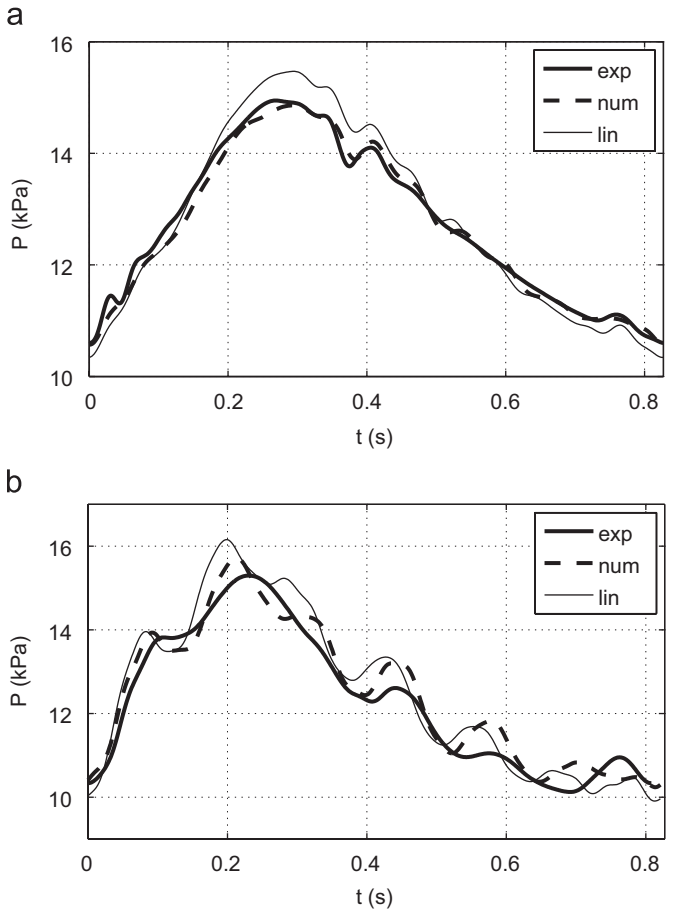

Fig. 7. Experimental and theoretical pressures waveforms at the inlet of the ascending aorta (segment 1) (a) and at the gastric artery (segment 21) (b). Theoretical pressures are calculated using the nonlinear (num) and linear (lin) formulations.

oscillations, since L adds to R_p a time-varying resistance whose value depends on the instantaneous outflow. On the other hand, a simulation using RCR models reduces the amplitude of the peripheral oscillations by smoothing the waveforms due to the windkessel effect. However, the decrease in amplitude is not sufficient to match the experimental measurements. Similar results are obtained in other terminal branches.

4. Discussion

We have presented a well-defined experimental 1:1 replica of the 37 largest systemic arteries in the human to test the numerical solution of the nonlinear, 1-D equations of pressure and flow pulse wave propagation. Following our previous research work in Segers and Verdonck (2000) and Alastruey (2006), this is the first attempt, to our knowledge, to test the accuracy of the 1-D formulation in the aorta and its branches up to the third generation of bifurcations. Although it is not an *in vivo* validation, it has the fundamental advantage of reducing the uncertainty of the parameters involved in the numerical algorithm. Unlike other *in vivo* validations (Olufsen et al., 2000; Steele et al., 2003), we have been able to directly measure all the parameters involved in the numerical algorithm. We first present some issues of the experimental modelling (Section 4.1) after which we discuss the numerical results (Section 4.2).

4.1. Experimental model

Although the experimental set-up is only an approximation to the human systemic circulation, it is able to reproduce pulse waveforms with significant physiological

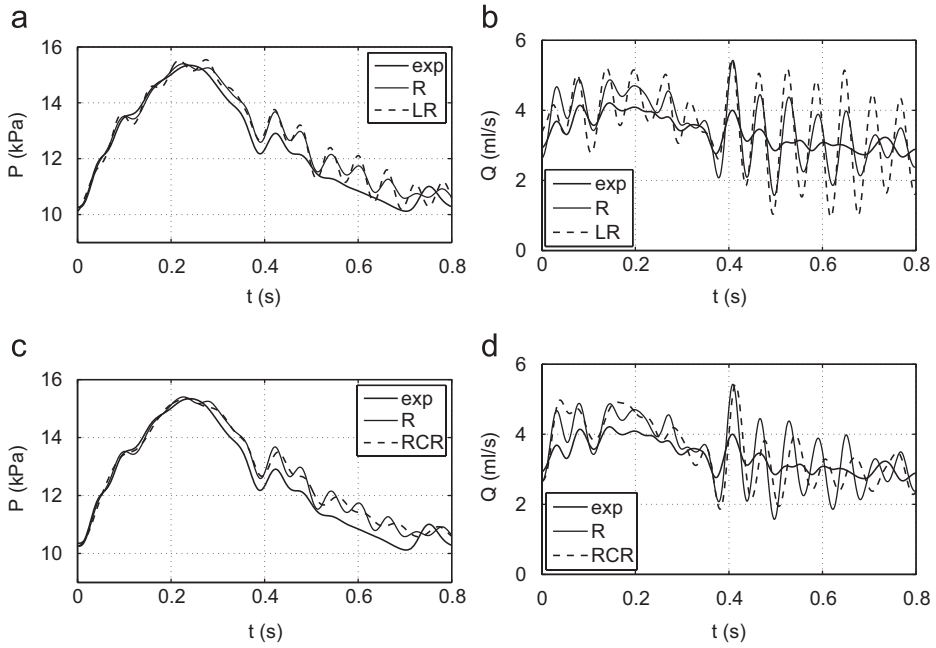

Fig. 8. Waveforms in the middle point of the left renal vessel (segment 24) comparing the experimental (exp) pressures (a,c) and flows (b,d) with their numerical predictions simulated using a single resistance (R), LR or RCR peripheral model.

features in the aortic vessels. However, waveforms become less 'physiological' as we approach the periphery. This is a consequence of the simple resistance boundary conditions used, which reflect any incoming wave without smoothing them. We did not incorporate peripheral compliances to allow accurate quantification of the parameters of the terminal boundary conditions. Reflected waves in the peripheral vessels do not have much effect on aortic flows because they get 'trapped' as they propagate towards the root of the system. The trapping occurs because the junctions are well-matched for forward waves, which means that they are not well-matched for backward waves (Sherwin et al., 2003b).

Accurate measurements of the parameters used in the numerical algorithm were obtained as described in Section 2.1.2. In addition, wave speeds were measured from the linear part of the experimental pressure–velocity loops (Khir et al., 2001). However, the wave speeds obtained from this technique were not reliable because of the lack of accuracy in the flow measurements in some locations. Accurate flow measurements rely upon close contact between the tube and the flow transducer, and since only five different sizes of transducers were available, some mismatches were inevitable at the 70 different measurement sites. This problem could have been avoided by suspending the model in a shallow water tank, which was impractical due to the scale of the model.

Interference from the main supply was sometimes present but was removed by a low-pass filter during the processing of the data. Some noise was introduced to the model through its contact with the table. This noise was relatively small and probably could have been avoided by suspending the model in a shallow water tank.

In the tensile tests negligible anisotropy was found among specimen sheets from the same sample cut at different angles (0°, 45° and 90°) with respect to the principal painting direction. A constant value of the Young's modulus was used for all vessels because the tensile tests showed insignificant variation with the vessel wall thickness.

4.2. Numerical model

Our results reveal the ability of the nonlinear, 1-D model to capture the main features of the experimental pulse waves, not only along the aorta, as has already been shown in Segers and Verdonck (2000) and Alastruey (2006), but also in more peripheral vessels, where the frequency of the numerical oscillations surprisingly mimics the experimental results. The average relative errors of the numerical predictions are smaller than 4% in pressure and 19% in the flow at all 70 locations studied. In general, relative errors are smaller at locations close to the inflow boundary condition, where the numerical flow matches its experimental counterpart. The larger relative errors in the flow predictions compared to their pressure counterparts can be explained because experimental flow measurements are less precise than experimental pressure measurements. As discussed in Section 4.1, this is primarily a consequence of the mismatch between the silicone tube and the flow transducer.

Discrepancies between experimental and numerical results arise from the uncertainties in the experimental measurements and the assumptions and simplifications of the 1-D formulation. We showed that these discrepancies cannot be a consequence of having neglected energy losses at junctions (Section 3.2). In addition, the higher amplitude of the numerical peripheral oscillations can only be partially explained by the presence of peripheral compliance in the overflow reservoirs (Section 3.3). The effect of neglecting the curvature of the vessels has not been analysed, although it should be secondary because of the geometry of our experimental system. Therefore, we conclude that the viscoelasticity of the silicone wall might have an important effect on damping peripheral oscillations, which will be addressed in a future work.

5. Conclusions

We have shown that the 1-D formulation captures the main features of pressure and flow pulse wave propagation in large vessels if accurate measurements of the geometry, wall compliance and boundary conditions of the system are provided. Our results show that energy losses at bifurcations have only a secondary effect on the blood flow in large arteries, and viscoelasticity might have a significant effect on the pulse waveforms in peripheral vessels. Accurate simultaneous pressure and flow measurements are essential to determine pulse wave speeds from pressure–flow loops.

This work is the first attempt to verify the nonlinear, 1-D formulation against a well-defined bifurcating network of vessels. We have demonstrated that the measured pressure and flow waveforms are accurately captured by the numerical simulation. Relative errors in pressure and the flow are smaller than 4% and 19%, respectively. We believe that the larger relative error in the flow can primarily be attributed to flow measurement uncertainty. The results presented here provide additional support for the use of the mathematical model, and its numerical simulation, to model clinically relevant problems (e.g., Stergiopulos et al., 1992; Smith et al., 2001; Steele et al., 2003; Franke et al., 2003; Alastruey et al., 2006, 2007a, b).

Conflict of Interest

There are no conflicts of interest between the authors of this paper and other external researchers or organisations that could have inappropriately influenced this work.

Acknowledgements

This work was partially supported by the EU RTN Haemodel Project (contract number HPRN-CT-2002-00270)

and an EPSRC Advanced Research Fellowship. The second author (J.A.) would like to acknowledge support from the Royal Academy of Engineering through an International Travel Grant. The technical staff from Ghent University at the CMBD Research Unit are greatly acknowledged for the construction of the experimental set-up and data-acquisition equipment.

References

Alastruey, J., 2006. Numerical modelling of pulse wave propagation in the cardiovascular system: development, validation and clinical applications, Ph.D. Thesis, Imperial College London, University of London.

Alastruey, J., Parker, K.H., Peiró, J., Sherwin, S.J., 2006. Can the modified Allen's test always detect sufficient collateral flow in the hand? A computational study. Computer Methods in Biomechanics and Biomedical Engineering 9, 353–361.

Alastruey, J., Moore, S.M., Parker, K.H., Peiró, J., David, T., Sherwin, S.J., 2007a. Reduced modelling of blood flow in the cerebral circulation: coupling 1-D, 0-D and cerebral auto-regulation models. International Journal for Numerical Methods in Fluids, accepted for publication.

Alastruey, J., Parker, K.H., Peiró, J., Byrd, S.M., Sherwin, S.J., 2007b. Modelling the circle of Willis to assess the effects of anatomical variations and occlusions on cerebral flows. Journal of Biomechanics 40, 1794–1805.

Blacher, J., Safar, M.E., 2005. Large-artery stiffness, hypertension and cardiovascular risk in older patients. Nature Clinical Practice Cardiovascular Medicine 2, 450–455.

Caro, C.G., Pedley, T.J., Schroter, R.C., Seed, W.A., 1978. The Mechanics of the Circulation. Oxford University Press, Oxford.

Cruickshank, K., Riste, L., Anderson, S.G., Wright, J.S., Dunn, G., Gosling, R.G., 2002. Aortic pulse-wave velocity and its relationship to mortality in diabetes and glucose intolerance. Circulation 106, 2085–2090.

Formaggia, L., Gerbeau, J.F., Nobile, F., Quarteroni, A., 2001. On the coupling of 3D and 1D Navier–Stokes equations for flow problems in compliant vessels. Computer Methods in Applied Mechanics and Engineering 191, 561–582.

Formaggia, L., Lamponi, D., Tuveri, M., Veneziani, A., 2006. Numerical modeling of 1D arterial networks coupled with a lumped parameters description of the heart. Computer Methods in Biomechanics and Biomedical Engineering 9, 273–288.

Franke, V.E., Parker, K.H., Wee, L.Y., Fisk, N.M., Sherwin, S.J., 2003. Time domain computational modeling of 1D arterial networks in monochorionic placentas. Mathematical Modelling and Numerical Analysis 37, 557–580.

Fujimoto, S., Mizuno, R., Saito, Y., Nakamura, S., 2004. Clinical application of wave intensity for the treatment of essential hypertension. Heart and Vessels 19, 19–22.

Gardel, A., 1957a. Les pertes de charge dans les écoulements au travers de branchements en té. Bulletin Technique de la Suisse Romande 9, 123–130.

Gardel, A., 1957b. Les pertes de charge dans les écoulements au travers de branchements en té. Bulletin Technique de la Suisse Romande 10, 143–148.

Karniadakis, G.E., Sherwin, S.J., 2003. Spectral/hp Element Methods for CFD. Oxford University Press, Oxford.

Khir, A.W., O'Brien, A., Gibbs, J.S.R., Parker, K.H., 2001. Determination of wave speed and wave separation in the arteries. Journal of Biomechanics 34, 1145–1155.

Olufsen, M.S., Peskin, C.S., Kim, W.Y., Pedersen, E.M., Nadim, A., Larsen, J., 2000. Numerical simulation and experimental validation of blood flow in arteries with structured-tree outflow conditions. Annals of Biomedical Engineering 28, 1281–1299.

Segers, P., Verdonck, P., 2000. Role of tapering in aortic wave reflection: hydraulic and mathematical model study. Journal of Biomechanics 33, 299–306.

Segers, P., Dubois, F., De Wachter, D., Verdonck, P., 1998. Role and relevancy of a cardiovascular simulator. Journal of Cardiovascular Engineering 3, 48–56.

Sherwin, S.J., Formaggia, L., Peiró, J., Franke, V., 2003a. Computational modelling of 1D blood flow with variable mechanical properties and its application to the simulation of wave propagation in the human arterial system. International Journal for Numerical Methods in Fluids 43, 673–700.

Sherwin, S.J., Franke, V., Peiró, J., Parker, K.H., 2003b. One-dimensional modelling of a vascular network in space-time variables. Journal of Engineering Mathematics 47, 217–250.

Smith, N.P., Pullan, A.J., Hunter, P.J., 2001. An anatomically based model of transient coronary blood flow in the heart. SIAM Journal on Applied Mathematics 62, 990–1018.

Steele, B.N., Wan, J., Ku, J.P., Hughes, T.J.R., Taylor, C.A., 2003. In vivo validation of a one-dimensional finite-element method for predicting blood flow in cardiovascular bypass grafts. IEEE Transactions in Biomedical Engineering 50, 649–656.

Stergiopulos, N., Young, D.F., Rogge, T.R., 1992. Computer simulation of arterial flow with applications to arterial and aortic stenoses. Journal of Biomechanics 25, 1477–1488.

Taylor, C.A., Draney, M.T., 2004. Experimental and computational methods in cardiovascular fluid mechanics. Annual Review of Fluid Mechanics 36, 197–231.

Wan, J., Steele, B.N., Spicer, S.A., Strohband, S., Feijoo, G.R., Hughes, T.J.R., Taylor, C.A., 2002. A one-dimensional finite element method for simulation-based medical planning for cardiovascular disease. Computer Methods in Biomechanics and Biomedical Engineering 5, 195–206.